Radiotherapy and Oncology 133 (2019) 77–86

Contents lists available at ScienceDirect

Radiotherapy and Oncology

journal homepage: www.thegreenjournal.com

Orignal Article

DNA damage response of clinical carbon ion versus photon radiation in human glioblastoma cells

Ramon Lopez Perez [a,*], Nils H. Nicolay [a,b,1], Jörg-Christian Wolf [a], Moritz Frister [a], Peter Schmezer [c], Klaus-Josef Weber [a], Peter E. Huber [a,*]

[a] CCU Molecular and Radiation Oncology, German Cancer Research Center and Department of Radiation Oncology, Heidelberg University Hospital; [b] Department of Radiation Oncology, Freiburg University Medical Center; and [c] Epigenomics and Cancer Risk Factors, German Cancer Research Center, Heidelberg, Germany

ARTICLE INFO

Article history:
Received 7 June 2018
Received in revised form 14 December 2018
Accepted 30 December 2018
Available online 17 January 2019

Keywords:
Carbon ion radiotherapy
Glioblastoma
DNA double-strand breaks
DNA repair
Homologous recombination

ABSTRACT

Background and purpose: Carbon ion radiotherapy is a promising therapeutic option for glioblastoma patients due to its high physical dose conformity and greater biological effectiveness than photons. However, the biological effects of carbon ion radiation are still incompletely understood. Here, we systematically compared the biological effects of clinically used carbon ion radiation to photon radiation with emphasis on DNA repair.

Materials and methods: Two human glioblastoma cell lines (U87 and LN229) were irradiated with carbon ions or photons and DNA damage response was systematically analyzed, including clonogenic survival, induction and repair of DNA double-strand breaks (DSBs), cell cycle arrest and apoptosis or autophagy. γH2AX foci were analyzed by flow cytometry, conventional light microscopy and 3D superresolution microscopy.

Results: DSBs were repaired delayed and with slower kinetics after carbon ions versus photons. Carbon ions caused stronger and longer-lasting cell cycle delays, predominantly in G2 phase, and a higher rate of apoptosis. Compared to photons, the effectiveness of carbon ions was less cell cycle-dependent. Homologous recombination (HR) appeared to be more important for DSB repair after carbon ions versus photons in phosphatase and tensin homolog (PTEN)-deficient U87 cells, as opposed to PTEN-proficient LN229 cells.

Conclusion: Carbon ions induced more severe DSB damage than photons, which was repaired less efficiently in both cell lines. Thus, carbon ion radiotherapy may help to overcome resistance mechanisms of glioblastoma associated with DNA repair for example in combination with repair pathway-specific drugs in the context of personalized radiotherapy.

Glioblastoma is the most frequent primary malignant human brain tumor with a dismal prognosis and a median survival of around 15 months under the current treatment regime – surgery followed by chemotherapy and photon radiotherapy [1]. Several recent large studies with the concept to add targeted drugs to conventional radiochemotherapy regimens have failed to substantially improve clinical results [2–4], highlighting the urgent need for alternative approaches. Carbon ion radiation has been demonstrated to exhibit a different radiobiology and higher anti-tumor effectiveness than photon radiation in several tumor and normal tissue models [5–13]. Carbon ion radiotherapy is currently being clinically investigated for treatment of several malignant tumors including glioblastoma [14–18].

Experimental studies suggested that the high linear energy transfer (LET) of heavy ions induces complex DNA damage patterns with difficult to repair clustered DNA double-strand breaks (DSB) [19–21]. Accumulating evidence suggests that high-LET radiation therefore triggers a differential DSB repair pathway choice com-

Abbreviations: ATM, ataxia telangiectasia mutated; BRCA1, Breast cancer type 1 susceptibility protein; CDK1, cyclin-dependent kinase 1; Chk2, checkpoint kinase 2; DAPI, 4′,6-Diamidin-2-phenylindol; DMEM, Dulbecco's Modified Eagle's Medium; DSB, DNA double-strand break; FCS, fetal calf serum; GAPDH, glyceraldehyde 3-phosphate dehydrogenase; HPRT1, hypoxanthine-guanine phosphoribosyltransferase; HR, homologous recombination; LET, linear energy transfer; NHEJ, non-homologous end-joining; PARP, poly(ADP-ribose) polymerase; PCR, polymerase chain reaction; PTEN, phosphatase and tensin homolog; RBE, relative biological effectiveness; RI, relative γH2AX induction; SOBP, spread-out Bragg peak; XRCC3, X-ray repair cross-complementing protein 3.

* Corresponding authors at: CCU Molecular and Radiation Oncology, German Cancer Research Center, Im Neuenheimer Feld 280, 69120 Heidelberg, Germany.

E-mail addresses: r.lopez@dkfz.de (R. Lopez Perez), p.huber@dkfz.de (P.E. Huber).

[1] Address b is the present address of this author; the work was done at address a.

https://doi.org/10.1016/j.radonc.2018.12.028
0167-8140/

pared to low-LET photon radiation [22,23]. Most of the studies in this context were performed with monoenergetic experimental heavy-ion beams within the Bragg peak, where the maximum LET is reached. However, for clinical ion beams multiple particle energies are combined to a spread-out Bragg peak (SOBP) to cover the whole tumor volume, and hence the average LET is smaller than for its monoenergetic pendant. Therefore, we have systematically investigated the biological effects of clinically used carbon ion versus photon radiation in human glioblastoma cells with emphasis on DSB induction, clustering and repair. DSBs were measured by detection of γH2AX, the Ser139-phosphorylated form of the histone H2AX [24–26]. Of note, we have extended the method spectrum for γH2AX foci analysis using superresolution microscopy, which has considerably improved the spatial resolution [5]. Furthermore, the potential shift between the two major repair pathways homologous recombination (HR) [27] and non-homologous end-joining (NHEJ) [28,29] was analyzed and we discuss potential clinical consequences for carbon ion radiotherapy of glioblastoma.

Materials and methods

Cell culture

U87-MG cells were cultured in Dulbecco's Modified Eagle's Medium (DMEM) supplemented with 10% fetal calf serum (FCS) and LN229 cells were cultured in DMEM supplemented with 5% FCS. Both cell lines were kept at 37 °C and 5% CO_2.

Irradiation

Cells were irradiated with 6 MV photons using a linear accelerator (ARTISTE, Siemens) or in rasterscan mode with 1.2–2.4 GeV carbon ions (8 mm spread-out Bragg peak) reaching an average linear energy transfer of ∼120 keV/μm at the Heidelberg Ion-Beam Therapy Center. In both cases, the beam was orthogonal to the cell layer and passed 3 cm of water-equivalent material before reaching the cells.

Immunofluorescent staining and microscopy

Cells on coverslips were irradiated, fixed with paraformaldehyde and permeabilized with 70% ethanol. Samples were washed and subsequently incubated with Image-iT FX signal enhancer, γH2AX antibody, AlexaFluor488-labeled secondary antibody and 4′,6-Diamidin-2-phenylindol (DAPI). The cells were embedded with Fluoromount G and imaged and analyzed using a motorized fluorescence microscope with Metafer software (MetaSystems). Three independent experiments were performed with 3 replicate samples and at least 500 cells were acquired from each sample. The sample medians were used for statistical analysis.

3D superresolution microscopy

Microscope slides were prepared as above and imaged with a structured illumination microscope providing superresolution for accurate measurement of the γH2AX foci volume. Image acquisition and reconstruction were done as previously described [5] and the foci volume was determined using the 3D object counter plugin in ImageJ.

Flow cytometry

Cells were irradiated and harvested with trypsin/ethylenediaminetetraacetic acid, fixed with paraformaldehyde and permeabilized with 70% ethanol. After washing, the cells were incubated with ribonuclease A, labeled antibodies against γH2AX (AlexaFluor488), phosphohistone-H3 (Ser10) (AlexaFluor555) and cleaved caspase-3 (Asp175) (AlexaFluor647), and DAPI. Samples were measured with a LSRII flow cytometer (BD) and data were analyzed using FlowJo 7.6.5 software (see details in Supplementary Methods). Three independent experiments were performed with U87 cells (1 with LN229) with 3 replicate samples and 10,000–20,000 cells were acquired from each sample. The sample medians were used for statistical analysis.

Western Blot analysis

Irradiated cells were lysed using the Qproteome Mammalian Protein Prep Kit (Qiagen), supplemented with Phosphatase Inhibitor Cocktail 2 and 3 (Sigma–Aldrich) and cOmplete Mini Protease Inhibitor (Roche Applied Sciences). Proteins were separated on acrylamide gels (5 μg/lane), transferred onto nitrocellulose (Amersham) or polyvinylidene difluoride membranes (Millipore) and probed with antibodies from sampler kits 'Autophagy', 'Cell Cycle Regulation II' and 'Double Strand Breaks Repair' plus anti-β-actin as loading control (Cell Signaling Technology). Protein bands were visualized on X-ray films using horseradish peroxidase-coupled secondary antibodies and an enhanced chemiluminescence kit (Cell Signaling Technology).

Knockdown of XRCC3

X-ray repair cross-complementing protein 3 (XRCC3) was knocked down in U87 and LN229 cells using siRNA-mediated RNAi technology. Transfection solutions containing no siRNA, non-targeting or XRCC3 siRNA (10 nM final concentration for U87 and 50 nM for LN229) and Dharmafect-I (Dharmacon) transfection reagent (0.5% final dilution) were prepared in OptiMEM (Thermo Scientific) and mixed 4:1 with antibiotic-free medium for transfection (see siRNA sequence and procedure details in Supplementary Methods).

Determination of XRCC3 knockdown efficiency

RNA was isolated from untreated, transfected or mock-transfected cells at 24, 48 and 72 hours after transfection, using the RNeasy Mini Kit (Qiagen). DNA was digested using the DNase I Kit (Qiagen). First strand cDNA synthesis was carried out with 500 ng of RNA using the SuperScript III reverse transcription kit, including mock reverse transcriptions as control for genomic DNA contamination. Quantitative real time polymerase chain reaction (PCR) was performed in triplicate using Universal probe technology and the LightCycler 480 (Roche). Two primer/probe sets were designed to cover expression of the 3 transcription variants of XRCC3 (see sequences in Supplementary Methods). Cp values were normalized against the mean of the three housekeeping genes glyceraldehyde 3-phosphate dehydrogenase (GAPDH), β-actin and hypoxanthine–guanine phosphoribosyltransferase (HPRT1). Optimal PCR efficiency of 2 was verified using a cDNA dilution series ranging from 1:10 to 1:10 000. Relative expression analysis was carried out with Excel.

Clonogenic survival

Colony formation assays were performed as previously described [30] and detailed in the Supplements. Survival curves were fitted according to the linear-quadratic model using Sigma Plot version 13 and the relative biological effectiveness of carbon ion radiation was calculated: RBE = (photon $dose_{X\%survival}$)/(carbon ion $dose_{X\%survival}$) with X = 10 and X = 50. All experiments were per-

formed 3 times (once for XRCC3 knockout experiments) with triplicate samples.

Statistics

Two-sided Student's *t* tests were performed with Excel to assess the significance of differences between two groups. For clonogenic survival data these tests were paired.

Results

Clonogenic survival assays in U87 cells showed that the relative biological effectiveness (RBE) of carbon ions versus photons ranged between 2.6 (at 10% survival) and 3.0 (at 50% survival) (Fig. 1a). To investigate if this range was reflected by the induction levels of DNA double-strand breaks (DSBs), we measured the dose–response of the DSB marker γH2AX. Linear dose–response curves were obtained for both radiation qualities, but carbon ions showed

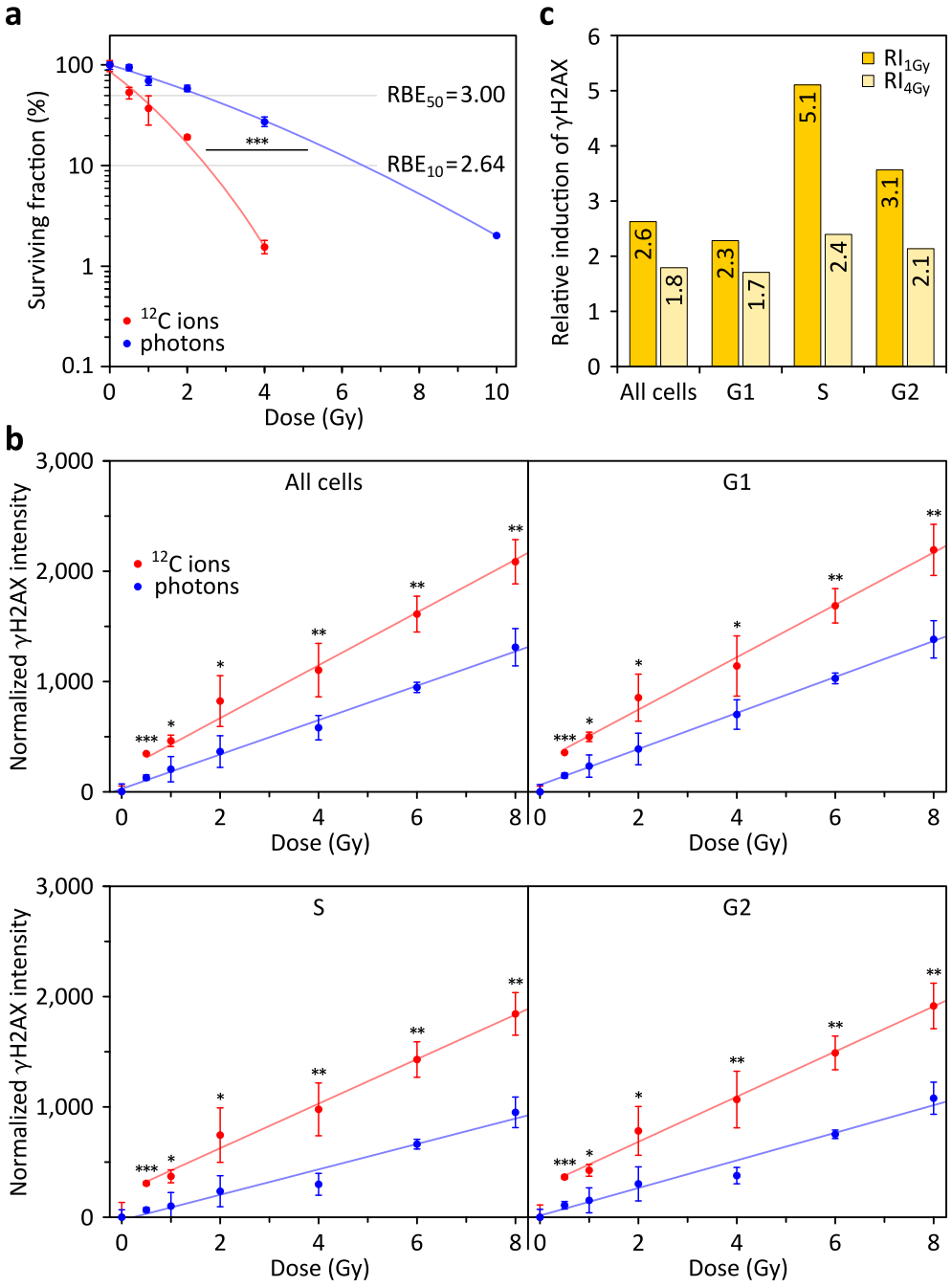

Fig. 1. Carbon ion radiation is more efficient in cell inactivation by induction of DNA double-strand breaks than photons. (a) Clonogenic survival of U87 cells. Symbols indicate mean and error bars SD values. Lines show fits according to the linear-quadratic model. The relative biological effectiveness of carbon ion radiation compared to photon radiation is indicated at a survival level of 50% (RBE_{50}) and 10% (RBE_{10}). (b) Cell cycle-specific induction of γH2AX measured by flow cytometry at 30 min after irradiation. For each sample the median fluorescence intensity was normalized to the relative DNA content in each cell cycle phase (G1 = 1.0, S = 1.5, G2 = 2.0) and control levels were subtracted. Symbols indicate mean and error bars SD values. Lines represent linear fits. (c) Relative induction of γH2AX by carbon ion compared to photon radiation as determined from the data shown in b at a dose of 1 Gy (RI_{1Gy}) and 4 Gy (RI_{4Gy}). $^{*}P < 0.05$, $^{**}P < 0.01$, $^{***}P < 0.001$ (two-sided Student's *t* test; in (a) the test was paired).

an over-proportional increase in γH2AX induction between 0 and 0.5 Gy (Fig. 1b). Therefore, the relative γH2AX induction (RI) of carbon ions versus photons at the same physical dose was higher for low doses (RI = 2.6 at 1 Gy vs. 1.8 at 4 Gy) for the whole cell population. This effect was even more pronounced in S and G2 phase (Fig. 1c). The slopes of the regression curves showed less variation between cell cycle phases for carbon ions, indicating less cell cycle dependence than for photons.

Microscopic evaluation of γH2AX in U87 cells (Fig. 2a) revealed a linear relationship between dose and fluorescence intensity (γH2AX molecules) for the foci (Fig. 2b), as well as for a weaker pan-nuclear γH2AX signal (Fig. 2c). In both cases, the dose response was markedly higher for carbon ion versus photon radiation, but the number of foci per nucleus was higher for photon radiation (Fig. 2d). Irrespective of the radiation quality, focus counts increased linearly up to 2 Gy and showed a saturation effect above. The foci size also reached a plateau at 2 Gy, but carbon ions induced much larger foci than photons (Fig. 2e). Time-course analyses confirmed that carbon ion-induced foci were larger for up to 48 h (Fig. 2f, Suppl. Fig. 1a), while the peak focus count was significantly higher for photon radiation (Fig. 2g, Suppl. Fig. 1b). Importantly, the larger foci size after carbon ion radiation was not due to bias from overlapping foci, as assessed by 3D superresolution microscopy with structured illumination (Fig. 3, Supplementary 360° movies). The qualitative differences between γH2AX foci induced by photons and carbon ions suggested that simple foci counting does not reflect the DSB induction level nor the relative biological effectiveness of carbon ion radiation. Instead, γH2AX intensity could be a better measure for the degree of DSB damage in cells.

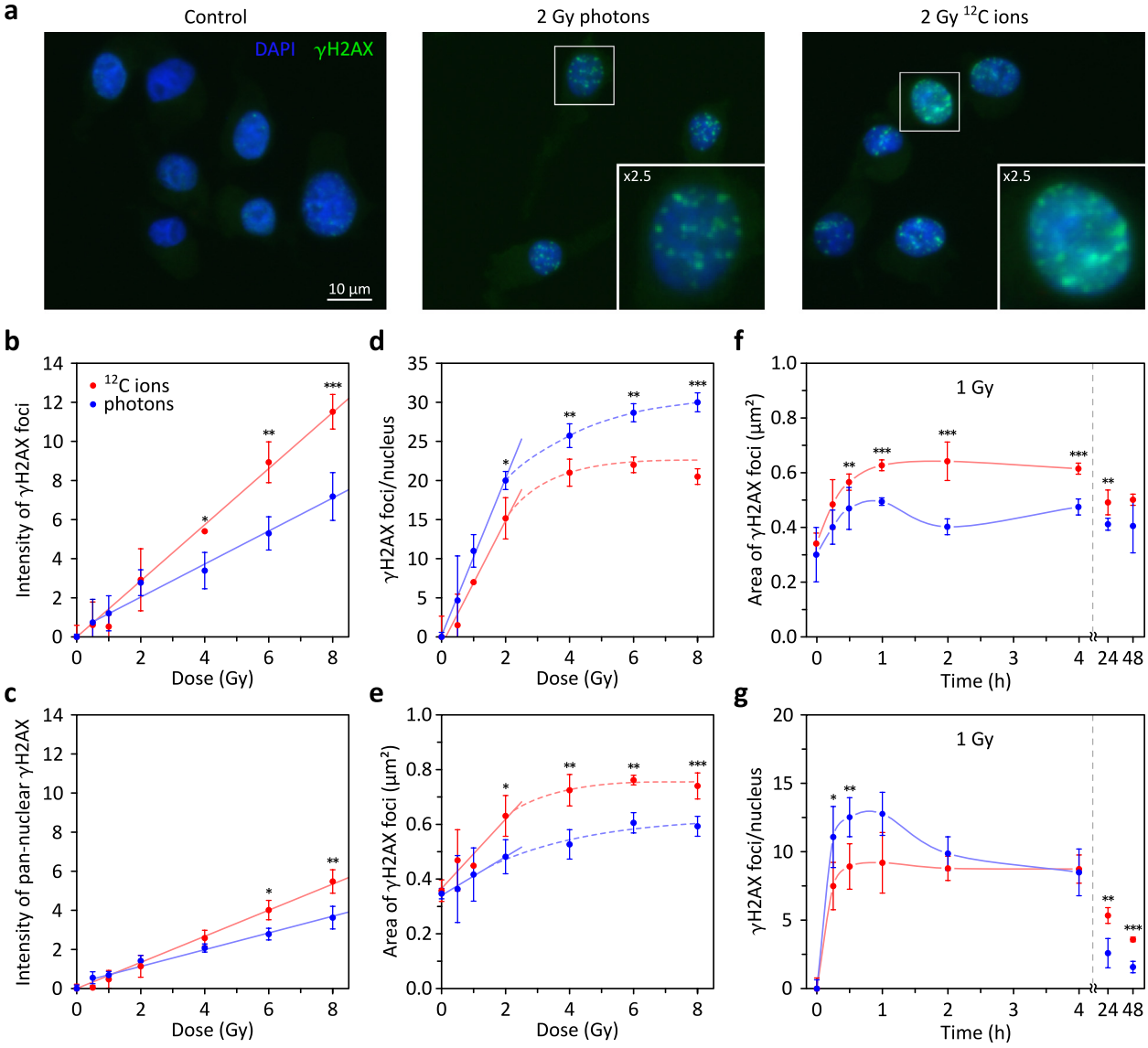

Fig. 2. Carbon ion radiation induces different patterns of DSB damage than photon radiation. Microscopic evaluation of γH2AX induction at 30 min after irradiation of U87 cells with different doses (a–e) and over time after 1 Gy (f–g) of carbon ion or photon radiation. (a) Example images. (b) Intensity of γH2AX foci above control level. (c, g) γH2AX focus count per nucleus above control level. (d) Area of γH2AX foci in µm^2. (e) Intensity of pan-nuclear γH2AX above control level. For each parameter the median was determined. Symbols indicate mean and error bars SD values. Solid lines represent linear fits and dashed lines exponential fits of the form (f(x) = y_{max} + W*e^(−x/s)). The broken lines in e and f do not represent fits. $^{*}P < 0.05$, $^{**}P < 0.01$, $^{***}P < 0.001$ (two-sided Student's t test).

Flow cytometric analysis in U87 and LN229 cells showed that the kinetics of γH2AX intensity (normalized to DNA content) were comparable in S and G2 phase and higher in G1 phase for 1 Gy (Fig. 4a) and 4 Gy (Suppl. Fig. 2a) of carbon ions. The same was true for photon radiation, except for LN229 cells irradiated with 1 Gy, where similar intensity levels were found across the cell cycle stages (Fig. 4a). Compared to photons, carbon ions induced higher peak levels that were reached later and declined slower. On average, the γH2AX peak levels induced by carbon ions were twice as high as for photons at 1 Gy in both U87 and LN229 cells (Fig. 4b). At 4 Gy the ratio was also 2 in LN229 cells and 1.5 in U87 cells (Suppl. Fig. 2b). Similar ratios were found for the decline time from peak to half value: it took 2.3x (U87)/2.2x (LN229) longer for carbon ions at 1 Gy (Fig. 4c) and 1.4x (U87)/1.5x (LN229) longer at 4 Gy (Suppl. Fig. 2c)).

Elevated γH2AX levels after 24 h and 48 h indicated residual DSBs considered as hard to repair and were comparable for photons and carbon ions after 1 Gy in U87 cells, but higher for carbon ions in LN229 cells. At 4 Gy carbon ions induced ~3-fold (U87) to ~4-fold (LN229) higher residual γH2AX levels after 48 h than photons, with the highest ratios being reached in G2 phase (Suppl. Fig. 2b). Together, these observations suggested that DSB repair was less efficient after carbon ion radiation versus photons.

Carbon ions also induced a more pronounced shift of the cell cycle distribution from G1 and S phase into G2 than photons in U87 and LN229 cells (Fig. 5a, Suppl. Fig. 3a), in agreement with inactivating phosphorylation of cyclin-dependent kinase 1 (CDK1) and expression of cyclins A2 and B1 (Fig. 5b, Suppl. Fig. 3b). Similar levels of activating checkpoint kinase 2 (Chk2) phosphorylation were observed for both types of radiation in both cell lines. The levels of p21 were also similar after carbon ion and photon radiation in U87 cells, while in LN229 cells carbon ions induced a more pronounced increase of p21 than photons. Coinciding with incomplete DSB repair and stronger cell cycle arrest, carbon ions led to higher rates of apoptosis in subG1 and caspase-3 analyses (Fig. 5c, Suppl. Fig. 3c) with >30% caspase-3-positive U87 cells (versus <10% after photons, $P < 0.001$) and >13% caspase-3-positive LN229 cells (versus 2.5% after photons, $P < 0.001$) at 4 Gy. Neither photons nor carbon ions induced any changes in the levels of the key proteins involved in autophagy, a possible rescue pathway alternative to apoptosis, as assessed in U87 cells (Suppl. Fig. 4).

A retarded DSB repair kinetic and prolonged cell cycle arrest in G2 phase suggested a stronger usage of the slow repair pathway of homologous recombination (HR) in carbon ion-irradiated cells. Accordingly, Western blot analyses confirmed that activating phosphorylation of the key HR promoting factor Breast cancer type 1 susceptibility protein (BRCA1) was stronger and lasted longer when U87 or LN229 cells were irradiated with carbon ions rather than photons (Fig. 6a, Suppl. Fig. 5a). To test the importance of HR for DSB repair in carbon ion-irradiated cells, we knocked down the recombinase XRCC3, which is essential for HR (Suppl. Fig. 6). Clonogenic survival assays showed a substantial increase of the RBE in knockdown versus mock-treated U87 cells, while LN229 cells showed the opposite behavior (Fig. 6b, c).

Discussion

Here we investigated mechanistic reasons for the elevated relative biological effectiveness (RBE) of clinical carbon ion radiation (with spread-out Bragg peak) versus photons in human glioblastoma cells. Carbon ions induced higher levels of the DNA double-strand break (DSB) marker γH2AX than photons and the induction was over-proportionally high for carbon ion doses below 0.5 Gy. Microscopic evaluation of γH2AX revealed that carbon ion radiation induced a smaller number of initial DSB foci than photons, but they were significantly larger and contained more γH2AX molecules than the foci induced by photons. Importantly, the larger foci size after carbon ion radiation was independently con-

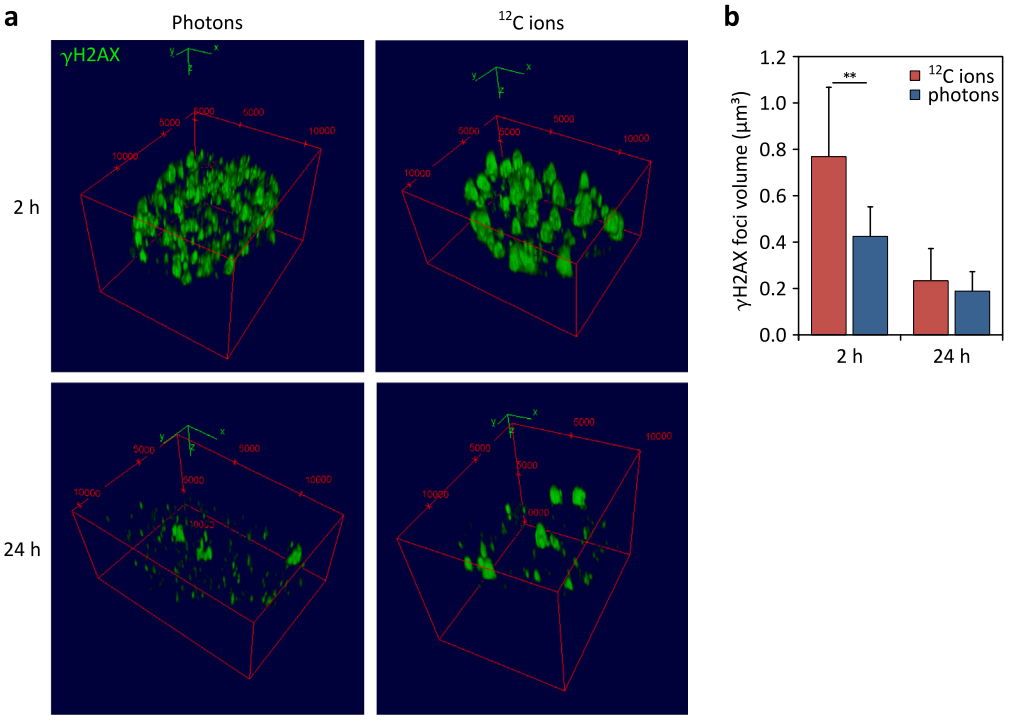

Fig. 3. Carbon ion radiation induces larger γH2AX foci than photon radiation. (a) 3D superresolution images of γH2AX foci at 2 and 24 h after irradiation of U87 cells with 4 Gy photons or carbon ions (scale in nm). (b) γH2AX foci volume (mean and SD). $^{*}P < 0.05$ (one-sided Student's *t* test).

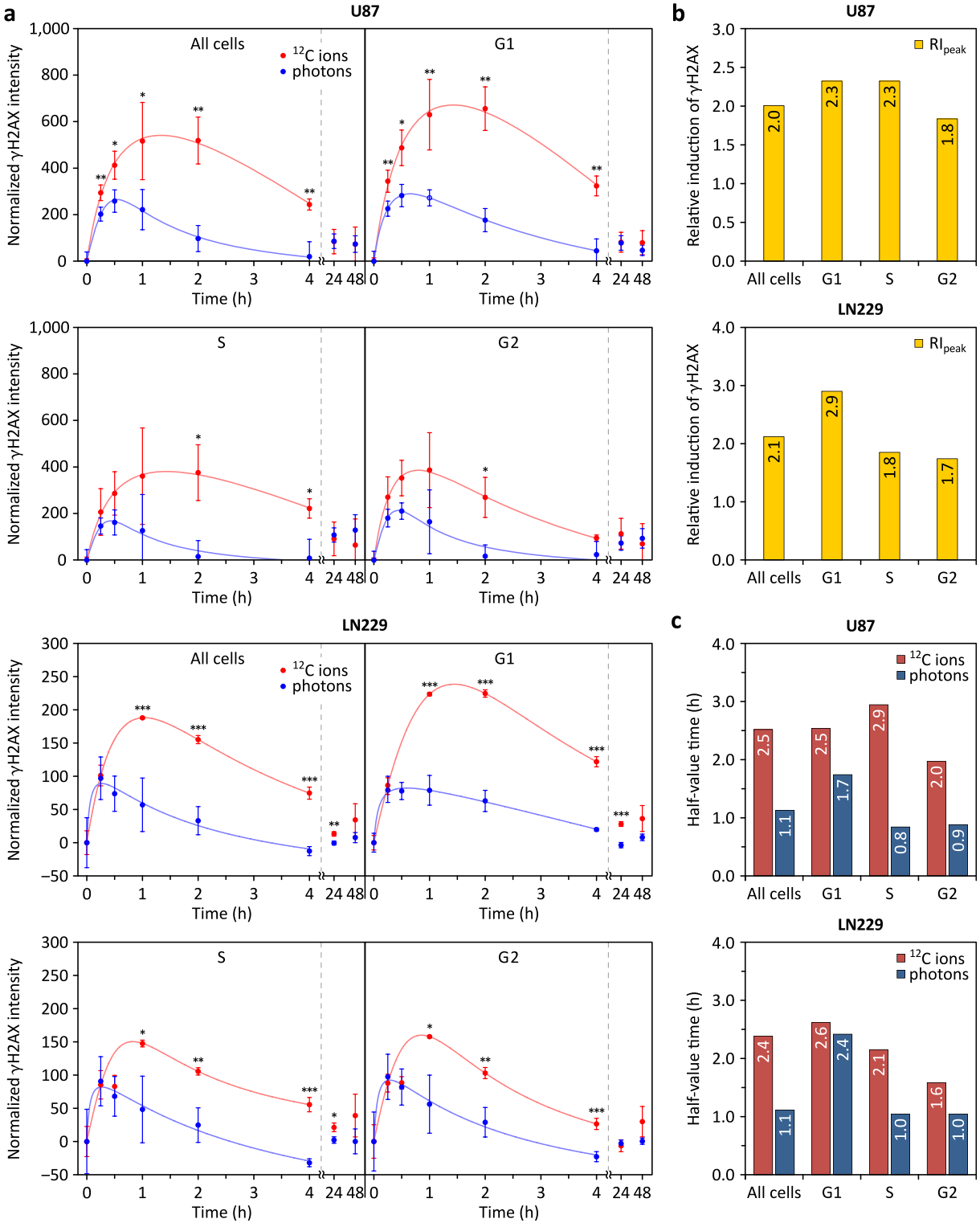

Fig. 4. Carbon ion-induced DSBs are repaired less efficiently than photon-induced DSBs. U87 and LN229 cells were irradiated with 1 Gy of carbon ion or photon radiation. (a) Cell cycle-specific induction of γH2AX measured by flow cytometry. For each sample the median fluorescence intensity was normalized to the relative DNA content in each cell cycle phase (G1 = 1.0, S = 1.5, G2 = 2.0) and control levels were subtracted. Symbols indicate mean and error bars SD values. Solid lines represent fits according to the function $I(t) = (p_1 * t^2 + p_2 * t)/(t^2 + q_1 * t + q_2) | t \geq 0,\ p_1 < 0,\ p_1, q_1, q_2 > 0$. (b) Relative induction of γH2AX at the peak level by carbon ion compared to photon radiation as determined from the data shown in (a). (c) Half-value time in hours as measured from the data in (a) (duration of the decrease of the γH2AX intensity from peak level to half of the peak value). $^{*}P < 0.05$, $^{**}P < 0.01$, $^{***}P < 0.001$ (two-sided Student's *t* test).

firmed using superresolution microscopy. Large γH2AX foci appear to be characteristic for high-LET radiation and have been linked to the induction of clustered DSB damage that is difficult to repair [31]. This is in accordance with the nearly linear clonogenic survival curves after carbon ion radiation, also suggesting nearly no sublethal damage and hence mostly complex DSBs. In addition to the foci, a weaker pan-nuclear γH2AX staining increased linearly with dose and was significantly stronger for carbon ions than pho-

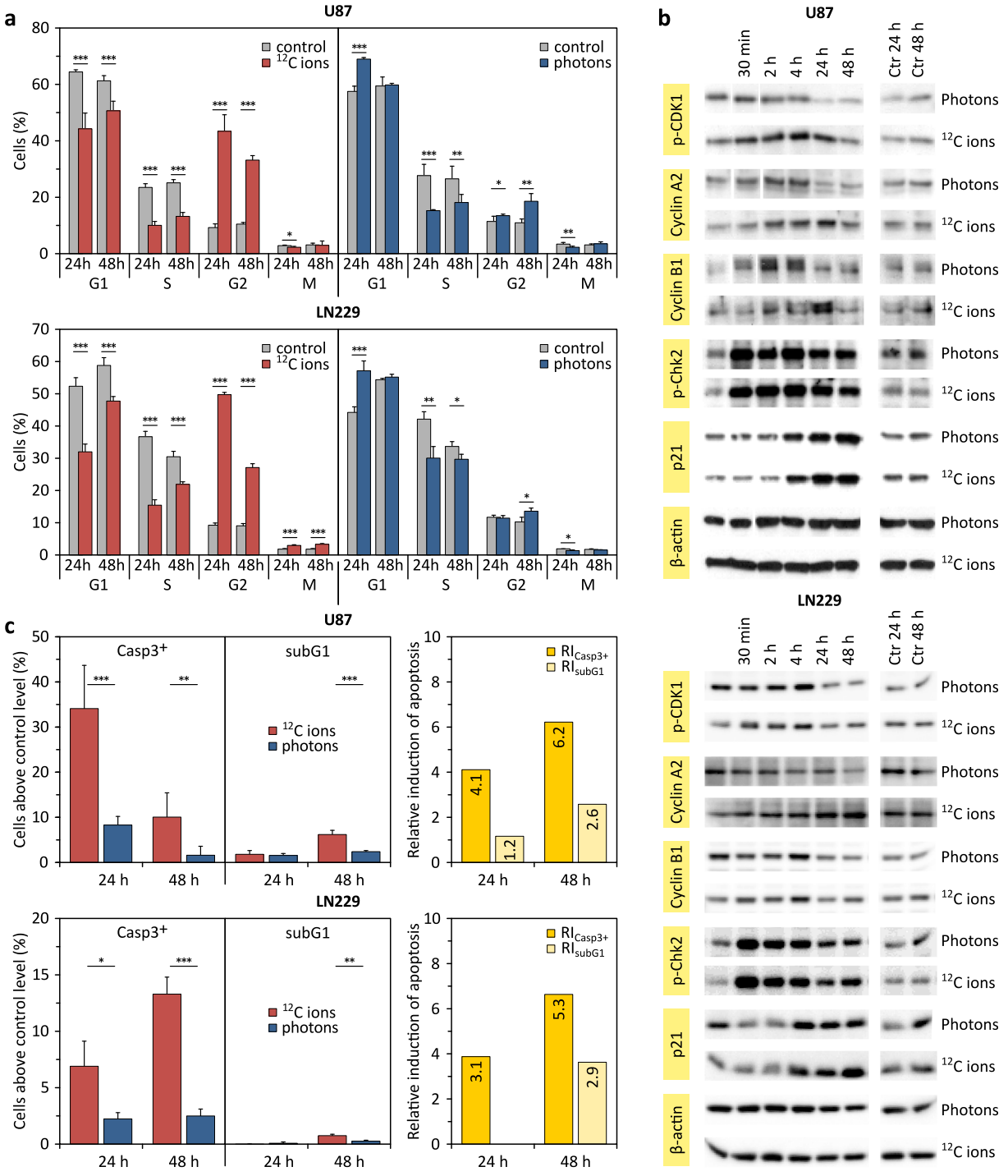

Fig. 5. Carbon ion radiation induces stronger G2 arrest and more apoptosis than photon radiation. U87 and LN229 cells were irradiated with 4 Gy of carbon ion or photon radiation. (a) Cell cycle distribution (mean and SD). (b) Western Blot analysis of cell cycle regulation proteins. (c) Apoptosis induction, as measured by caspase-3 and subG1 positive cells (mean and SD).

tons. Pan-nuclear γH2AX induction has also been linked to clustered DSB damage [32], further stressing the role of complex DNA lesions for the increased RBE of carbon ion radiation.

Cell cycle-specific analyses of γH2AX induction showed that the effectiveness of carbon ion radiation was less dependent on the cell cycle stage than for photon radiation. DSB repair was delayed and progressed slower when cells were irradiated with carbon ions. In addition, residual γH2AX foci at 24 h and 48 h after irradiation indicated that carbon ions generated significantly more persistent DNA damage than photons. This led to stronger and prolonged cell cycle arrest in G2 phase and a higher rate of apoptosis after carbon ion irradiation. The three-fold increase in U87 subG1 cells by carbon ion versus photon radiation was in good accordance with the RBE determined by clonogenic survival assays. The percentage of subG1 cells was considerably smaller than the percentage of caspase-3-positive U87 as well as LN229 cells, probably indicating that other cell fates like mitotic catastrophe or senescence may also contribute to radiation-induced cell inactivation in

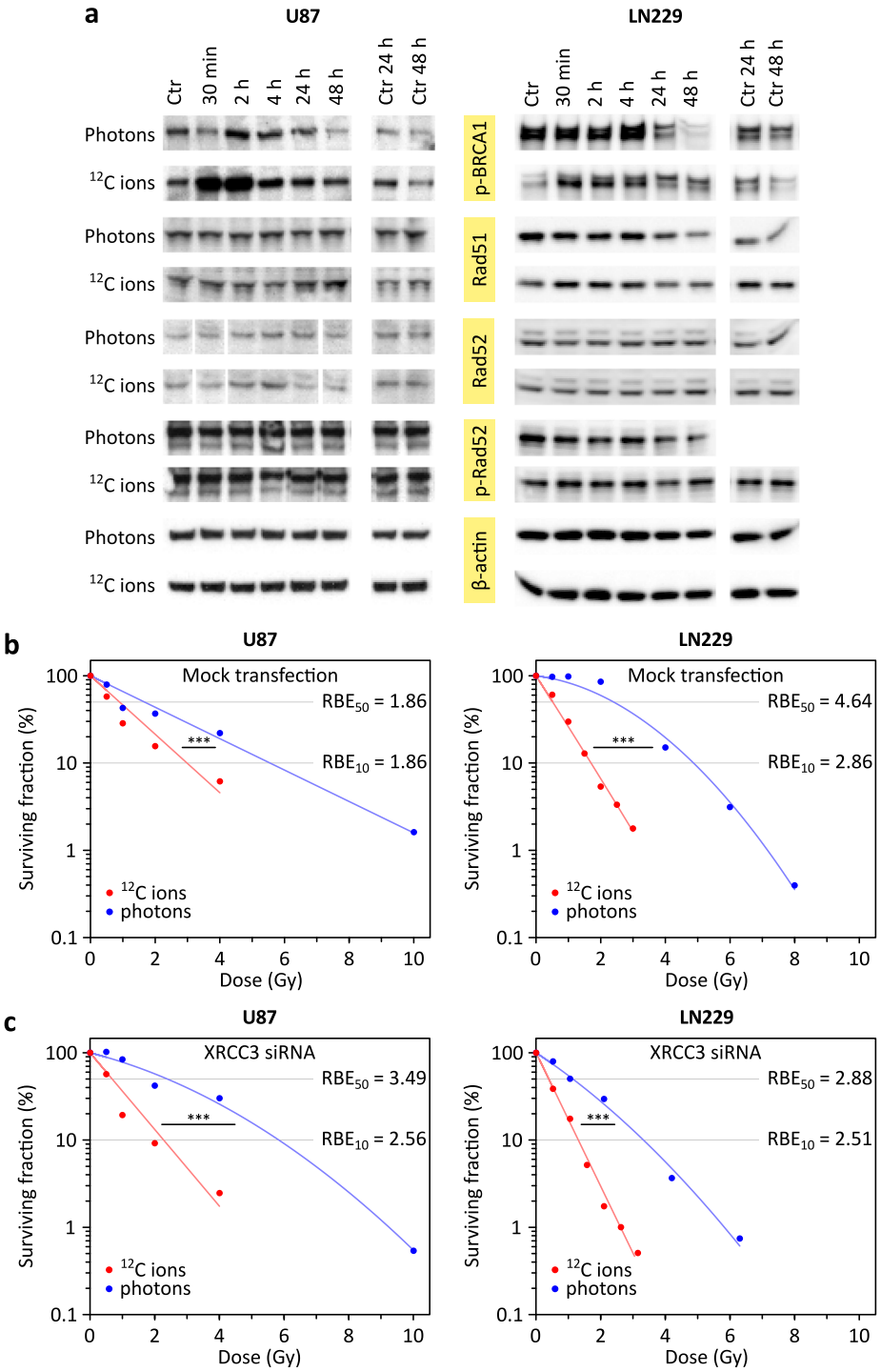

Fig. 6. Importance of homologous recombination for repair of carbon ion-induced DSBs versus photon-induced DSBs. (a) Western Blot analysis of homologous recombination repair proteins after irradiation of U87 and LN229 cells with 1 Gy of carbon ion versus photon radiation. (b) Clonogenic survival assay of mock transfected or (c) XRCC3 knockdown cells. The graphs show the mean surviving fraction from 3 replicates and fits according to the linear-quadratic model. The relative biological effectiveness of carbon ion radiation compared to photon radiation is indicated at a survival level of 50% (RBE_{50}) and 10% (RBE_{10}).

glioblastoma. Autophagy as one potential resistance mechanism could be excluded to play an important role after either photon or carbon ion radiation in U87 cells.

The success of DSB repair is key to cell survival and the retarded repair kinetics associated with carbon ion radiation suggested enhanced utilization of the slow homologous recombination (HR) pathway. Protein data supported this hypothesis for U87 as well as LN229 cells. HR knockdown experiments confirmed that HR was more relevant for repair of DSBs induced by carbon ions versus photons in U87 cells, in agreement with reports in Chinese hamster cells [22] and mature as well as immature cells of the hematopoietic system [23]. A potential explanation for the particular importance of HR after carbon ion radiation is the inefficient repair of densely clustered DSBs by non-homologous end-joining (NHEJ): Ku proteins, which initiate NHEJ, fail to bind to small DNA fragments occurring at clustered DSB sites [33]. Although Ku-independent alternative end joining pathways exist, they are even more error-prone than the canonical NHEJ pathway [21,34].

Interestingly, LN229 cells showed no enhanced sensitivity to carbon ion radiation when HR was knocked down by siRNA directed against XRCC3. In fact, the RBE of carbon ions versus photons even decreased. We cannot completely exclude off-target effects of the siRNA, but it is more likely that Ku-independent alternative NHEJ repair caused this result. These pathways are normally suppressed when HR is not compromised and may have been activated by the HR knockdown in LN229 cells. It is important to mention that here we have analyzed the relevance of the HR pathway for repair of carbon ion-induced DNA damage in comparison to photon-induced damage, and not the contribution of HR to the overall DNA repair.

The genetic differences that might be responsible for the differential effect of HR knockdown on RBE between LN229 and U87 cells include their phosphatase and tensin homolog (PTEN) status: LN229 cells are PTEN-proficient, while in U87 cells PTEN is homozygously defective. PTEN-deficiencies are common in glioblastoma and are known to increase the radioresistance of the tumor [35–37] by constitutive activation of the phosphatidylinositol 3-kinase/Akt pathway [38]. This induces several resistance mechanisms including the promotion of fast DSB repair by Ku-dependent NHEJ [39,40] and suppression of the slow HR pathway [41] which may have contributed to the differential response of LN229 and U87 cells to carbon ions versus photons.

Hence, carbon ion radiotherapy could be particularly useful to circumvent this resistance mechanism in PTEN-deficient glioblastoma by impeding NHEJ and taking advantage of HR suppression. Following the concept of synthetic lethality, it could be beneficial to combine carbon ion radiotherapy with drugs targeting DSB repair, such as ataxia telangiectasia mutated (ATM) or poly(ADP-ribose) polymerase (PARP) inhibitors that have been shown to strongly aggravate HR-deficiencies in glioblastoma and other cancers [41–43]. On the other hand, DSB repair is not the only mechanism responsible for radioresistance [44]. Aside from glioblastoma cell intrinsic aspects, the tumor microenvironment plays an important role in radioresistance and clinical countermeasures [45]. Also normal cells and their plasticity upon radiation may contribute to the differential response to carbon ions versus photons in situ [30], and the immune system could play a role in this context as well.

In summary, we have shown important differential aspects of clinical carbon ion versus photon radiation, namely that carbon ions induced more severe DSB damage that was repaired less efficiently, leading to prolonged cell cycle delays and increased apoptosis in two human glioblastoma cell lines. Furthermore, the HR pathway was more relevant for DSB repair after carbon ion versus photon radiation in PTEN-deficient U87 cells, potentially inferring personalized radiotherapeutic options in glioblastoma patients based on genetic analyses.

Author contributions

R.L.P. designed the study, designed and performed experiments, developed data evaluation tools, analyzed data and wrote the paper; N.H.N. helped interpreting data and writing the manuscript; J.-C.W. and M.F. performed experiments and analyzed data; P.S. and K.-J.W. helped designing the study and interpreting data. P.E. H. helped designing the study, interpreting data, writing the manuscript, and supervised the study. All authors revised the manuscript.

Competing financial interests

The authors declare no competing financial interests.

Conflicts of interest

None.

Funding

This work was supported in part by grants from Kompetenzverbund Strahlenforschung (KVSF) of the German Ministries for Education, Research and Environment, Bundesministerien für Bildung, Forschung und Umwelt (BMBF/BMU) [03NUK004A,C]. Funding for open access charge: Institutional funds.

Acknowledgements

We thank Reinhard Gliniorz, Peter Waas, Otto Zelezny, Steffen Schmitt and Wahyu Hadiwikarta from the German Cancer Research Center for their support with γH2AX foci evaluation, qPCR based expression profiling, flow cytometry and data analysis. We also thank Thuy Trinh from the Heidelberg University Clinic for her help with clonogenic assays.

Appendix A. Supplementary data

Supplementary data to this article can be found online at https://doi.org/10.1016/j.radonc.2018.12.028.

References

[1] Stupp R, Mason WP, van den Bent MJ, Weller M, Fisher B, Taphoorn MJB, et al. Radiotherapy plus concomitant and adjuvant temozolomide for glioblastoma. N Engl J Med 2005;352:987–96. https://doi.org/10.1056/NEJMoa043330.
[2] Stupp R, Hegi ME, Gorlia T, Erridge SC, Perry J, Hong Y-K, et al. Cilengitide combined with standard treatment for patients with newly diagnosed glioblastoma with methylated MGMT promoter (CENTRIC EORTC 26071–22072 study): a multicentre, randomised, open-label, phase 3 trial. Lancet Oncol 2014;15:1100–8. https://doi.org/10.1016/S1470-2045(14)70379-1.
[3] Gilbert MR, Dignam JJ, Armstrong TS, Wefel JS, Blumenthal DT, Vogelbaum MA, et al. A randomized trial of bevacizumab for newly diagnosed glioblastoma. N Engl J Med 2014;370:699–708. https://doi.org/10.1056/NEJMoa1308573.
[4] Happold C, Gorlia T, Chinot O, Gilbert MR, Nabors LB, Wick W, et al. Does valproic acid or levetiracetam improve survival in glioblastoma? A pooled analysis of prospective clinical trials in newly diagnosed glioblastoma. J Clin Oncol 2016;34:731–9. https://doi.org/10.1200/JCO.2015.63.6563.
[5] Lopez Perez R, Best G, Nicolay NH, Greubel C, Rossberger S, Reindl J, et al. Superresolution light microscopy shows nanostructure of carbon ion radiation-induced DNA double-strand break repair foci. FASEB J 2016;30:2767–76. https://doi.org/10.1096/fj.201500106R.
[6] Frrandone S, Magné N, Battiston-Montagne P, Hau-Desbat N-H, Diaz O, Beuve M, et al. Cellular and molecular portrait of eleven human glioblastoma cell lines under photon and carbon ion irradiation. Cancer Lett 2015;360:10–6. https://doi.org/10.1016/j.canlet.2015.01.025.
[7] Jin X, Li F, Zheng X, Liu Y, Hirayama R, Liu X, et al. Carbon ions induce autophagy effectively through stimulating the unfolded protein response and subsequent inhibiting Akt phosphorylation in tumor cells. Sci Rep 2015;5:13815. https://doi.org/10.1038/srep13815.
[8] Walenta S, Mueller-Klieser W. Differential superiority of heavy charged-particle irradiation to X-rays: studies on biological effectiveness and side effect mechanisms in multicellular tumor and normal tissue models. Front Oncol 2016;6:30. https://doi.org/10.3389/fonc.2016.00030.
[9] Glowa C, Karger CP, Brons S, Zhao D, Mason RP, Huber PE, et al. Carbon ion radiotherapy decreases the impact of tumor heterogeneity on radiation response in experimental prostate tumors. Cancer Lett 2016;378:97–103. https://doi.org/10.1016/j.canlet.2016.05.013.
[10] Glowa C, Peschke P, Brons S, Neels OC, Kopka K, Debus J, et al. Carbon ion radiotherapy: impact of tumor differentiation on local control in experimental prostate carcinomas. Radiat Oncol 2017;12:174. https://doi.org/10.1186/s13014-017-0914-9.
[11] Saager M, Glowa C, Peschke P, Brons S, Scholz M, Huber PE, et al. Carbon ion irradiation of the rat spinal cord: dependence of the relative biological effectiveness on linear energy transfer. Int J Radiat Oncol Biol Phys 2014;90:63–70. https://doi.org/10.1016/j.ijrobp.2014.05.008.
[12] Peschke P, Karger CP, Scholz M, Debus J, Huber PE. Relative biological effectiveness of carbon ions for local tumor control of a radioresistant prostate carcinoma in the rat. Int J Radiat Oncol Biol Phys 2011;79:239–46. https://doi.org/10.1016/j.ijrobp.2010.07.1976.
[13] Durante M. New challenges in high-energy particle radiobiology. Br J Radiol 2014;87:20130626. https://doi.org/10.1259/bjr.20130626.

[14] Combs SE, Hartmann C, Nikoghosyan A, Jäkel O, Karger CP, Haberer T, et al. Carbon ion radiation therapy for high-risk meningiomas. Radiother Oncol 2010;95:54–9. https://doi.org/10.1016/j.radonc.2009.12.029.
[15] Uhl M, Mattke M, Welzel T, Roeder F, Oelmann J, Habl G, et al. Highly effective treatment of skull base chordoma with carbon ion irradiation using a raster scan technique in 155 patients: First long-term results. Cancer 2014;120:3410–7. https://doi.org/10.1002/cncr.28877.
[16] Adeberg S, Harrabi SB, Verma V, Bernhardt D, Grau N, Debus J, et al. Treatment of meningioma and glioma with protons and carbon ions. Radiat Oncol 2017;12:193. https://doi.org/10.1186/s13014-017-0924-7.
[17] Mattke M, Vogt K, Bougatf N, Welzel T, Oelmann-Avendano J, Hauswald H, et al. High control rates of proton- and carbon ion-beam treatment with intensity-modulated active raster scanning in 101 patients with skull base chondrosarcoma at the Heidelberg Ion Beam Therapy Center. Cancer 2018. https://doi.org/10.1002/cncr.31298.
[18] El Shafie RA, Czech M, Kessel KA, Habermehl D, Weber D, Rieken S, et al. Clinical outcome after particle therapy for meningiomas of the skull base: toxicity and local control in patients treated with active rasterscanning. Radiat Oncol 2018;13:54. https://doi.org/10.1186/s13014-018-1002-5.
[19] Sekine E, Okada M, Matsufuji N, Yu D, Furusawa Y, Okayasu R. High LET heavy ion radiation induces lower numbers of initial chromosome breaks with minimal repair than low LET radiation in normal human cells. Mutat Res 2008;652:95–101. https://doi.org/10.1016/j.mrgentox.2008.01.003.
[20] Stenerlow B, Hoglund E, Carlsson J. DNA fragmentation by charged particle tracks. Adv Sp Res 2002;30:859–63.
[21] Schipler A, Mladenova V, Soni A, Nikolov V, Saha J, Mladenov E, et al. Chromosome thripsis by DNA double strand break clusters causes enhanced cell lethality, chromosomal translocations and 53BP1-recruitment. Nucleic Acids Res 2016;44:7673–90. https://doi.org/10.1093/nar/gkw487.
[22] Gerelchuluun A, Manabe E, Ishikawa T, Sun L, Itoh K, Sakae T, et al. The major DNA repair pathway after both proton and carbon-ion radiation is NHEJ, but the HR pathway is more relevant in carbon ions. Radiat Res 2015;183:345–56. https://doi.org/10.1667/RR13904.1.
[23] Rall M, Kraft D, Volcic M, Cucu A, Nasonova E, Taucher-Scholz G, et al. Impact of charged particle exposure on homologous DNA double-strand break repair in human blood-derived cells. Front Oncol 2015;5:250. https://doi.org/10.3389/fonc.2015.00250.
[24] Rogakou EP, Boon C, Redon C, Bonner WM. Megabase chromatin domains involved in DNA double-strand breaks in vivo. J Cell Biol 1999;146:905–15. https://doi.org/10.1083/jcb.146.5.905.
[25] Huang X, Darzynkiewicz Z. Cytometric assessment of histone H2AX phosphorylation: a reporter of DNA damage. Methods Mol Biol 2006;314:73–80. https://doi.org/10.1385/1-59259-973-7:073.
[26] Nakamura A, Sedelnikova OA, Redon C, Pilch DR, Sinogeeva NI, Shroff R, et al. Techniques for gamma-H2AX detection. Methods Enzym 2006;409:236–50. https://doi.org/10.1016/S0076-6879(05)09014-2.
[27] Mimitou EP, Symington LS. DNA end resection: Many nucleases make light work. DNA Repair (Amst) 2009;8:983–95. https://doi.org/10.1016/j.dnarep.2009.04.017.
[28] van Gent DC, van der Burg M. Non-homologous end-joining, a sticky affair. Oncogene 2007;26:7731–40. https://doi.org/10.1038/sj.onc.1210871.
[29] Lieber MR. The mechanism of double-strand DNA break repair by the nonhomologous DNA end-joining pathway. Annu Rev Biochem 2010;79:181–211. https://doi.org/10.1146/annurev.biochem.052308.093131.
[30] Nicolay NH, Liang Y, Lopez Perez R, Bostel T, Trinh T, Sisombath S, et al. Mesenchymal stem cells are resistant to carbon ion radiotherapy. Oncotarget 2015;6:2076–87.
[31] Costes SV, Boissière A, Ravani S, Romano R, Parvin B, Barcellos-Hoff MH. Imaging features that discriminate between foci induced by high- and low-LET radiation in human fibroblasts. Radiat Res 2006;165:505–15. https://doi.org/10.1667/RR3538.1.
[32] Meyer B, Voss K-O, Tobias F, Jakob B, Durante M, Taucher-Scholz G. Clustered DNA damage induces pan-nuclear H2AX phosphorylation mediated by ATM and DNA-PK. Nucleic Acids Res 2013;41:6109–18. https://doi.org/10.1093/nar/gkt304.
[33] Wang H, Wang Y. Heavier ions with a different linear energy transfer spectrum kill more cells due to similar interference with the Ku-dependent DNA repair pathway. Radiat Res 2014;182. https://doi.org/10.1667/RR13857.1.
[34] Schipler A, Iliakis G. DNA double-strand-break complexity levels and their possible contributions to the probability for error-prone processing and repair pathway choice. Nucleic Acids Res 2013;41:7589–605. https://doi.org/10.1093/nar/gkt556.
[35] Xiao A, Yin C, Yang C, Di Cristofano A, Pandolfi PP, Van Dyke T. Somatic induction of pten loss in a preclinical astrocytoma model reveals major roles in disease progression and avenues for target discovery and validation. Cancer Res 2005;65:5172–80. https://doi.org/10.1158/0008-5472.CAN-04-3902.
[36] Furnari FB, Fenton T, Bachoo RM, Mukasa A, Stommel JM, Stegh A, et al. Malignant astrocytic glioma: genetics, biology, and paths to treatment. Genes Dev 2007;21:2683–710. https://doi.org/10.1101/gad.1596707.
[37] Duan S, Yuan G, Liu X, Ren R, Li J, Zhang W, et al. PTEN deficiency reprogrammes human neural stem cells towards a glioblastoma stem cell-like phenotype. Nat Commun 2015;6:10068. https://doi.org/10.1038/ncomms10068.
[38] Kao GD, Jiang Z, Fernandes AM, Gupta AK, Maity A. Inhibition of phosphatidylinositol-3-OH kinase/Akt signaling impairs DNA repair in glioblastoma cells following ionizing radiation. J Biol Chem 2007;282:21206–12. https://doi.org/10.1074/jbc.M703042200.
[39] Xu N, Lao Y, Zhang Y, Gillespie DA. Akt: a double-edged sword in cell proliferation and genome stability. J Oncol 2012;2012:1–15. https://doi.org/10.1155/2012/951724.
[40] Toulany M, Lee K-J, Fattah KR, Lin Y-F, Fehrenbacher B, Schaller M, et al. Akt promotes post-irradiation survival of human tumor cells through initiation, progression, and termination of DNA-PKcs-dependent DNA double-strand break repair. Mol Cancer Res 2012;10:945–57. https://doi.org/10.1158/1541-7786.MCR-11-0592.
[41] McEllin B, Camacho CV, Mukherjee B, Hahm B, Tomimatsu N, Bachoo RM, et al. PTEN loss compromises homologous recombination repair in astrocytes: Implications for glioblastoma therapy with temozolomide or poly(ADP-Ribose) polymerase inhibitors. Cancer Res 2010;70:5457–64. https://doi.org/10.1158/0008-5472.CAN-09-4295.
[42] Hengel SR, Spies MA, Spies M. Small-molecule inhibitors targeting DNA repair and DNA repair deficiency in research and cancer therapy. Cell Chem Biol 2017;24:1101–19. https://doi.org/10.1016/j.chembiol.2017.08.027.
[43] Majuelos-Melguizo J, Rodríguez MI, López-Jiménez L, Rodríguez-Vargas JM, Martín-Consuegra JMM, Serrano-Sáenz S, et al. PARP targeting counteracts gliomagenesis through induction of mitotic catastrophe and aggravation of deficiency in homologous recombination in PTEN-mutant glioma. Oncotarget 2015;6:4790–803. https://doi.org/10.18632/oncotarget.2993.
[44] Osswald M, Jung E, Sahm F, Solecki G, Venkataramani V, Blaes J, et al. Brain tumour cells interconnect to a functional and resistant network. Nature 2015;528:93–8. https://doi.org/10.1038/nature16071.
[45] Zhang M, Kleber S, Röhrich M, Timke C, Han N, Tuettenberg J, et al. Blockade of TGF-β signaling by the TGFβR-I kinase inhibitor LY2109761 enhances radiation response and prolongs survival in glioblastoma. Cancer Res 2011;71:7155–67. https://doi.org/10.1158/0008-5472.CAN-11-1212.